Nano Communication Networks ▮ (▮▮▮▮) ▮▮▮–▮▮▮

Contents lists available at ScienceDirect

Nano Communication Networks

journal homepage: www.elsevier.com/locate/nanocomnet

Modulation and rate adaptation algorithms for terahertz channels

Farnoosh Moshir*, Suresh Singh

Department of Computer Science, Portland State University, Portland, OR 97207, United States

ARTICLE INFO

Article history:
Received 4 January 2016
Received in revised form
17 June 2016
Accepted 12 July 2016
Available online xxxx

Keywords:
THz channel model
THz pulsed signal
THz continuous signal
Adaptation rate

ABSTRACT

The ever increasing demand for higher wireless data rates has led to the development of new techniques to increase spectrum efficiency. However, the limited bandwidth of the frequency bands that are currently used for wireless communication bounds the maximum data rate possible. In the past few years, researchers have developed new devices that work as Terahertz (THz) transmitters and receivers. The development of these devices and the large available bandwidth of the THz band is a possible solution to this ever increasing demand. However, THz communication is still in its infancy and more research needs to be done to bring THz technology into every day life.

This paper considers two specific problems — modulation of terahertz pulses and rate adaptation for terahertz communication systems. We describe a pulse modulation technique where multiple symbols are transmitted in each pulse. The technique is shown to achieve terabit/sec datarates. Subsequently, we examine the problem of rate adaptation which is significant at these frequencies due to the high distance based attenuation. Algorithms are presented to fairly share the channel among multiple users located at different distances from the access point. The research is based on simulations in Matlab and the channel model used is based on our own measurements using a time-domain terahertz system. The channel model is also presented in this paper.

1. Introduction

The demand for higher data rates is ever increasing and is unlikely to stabilize anytime soon. This trend is driven by increasing number of deployed devices providing content-rich data to users and the demand from users for greater download speeds, anywhere and anytime. For example, the Japanese government estimated that the annual growth rate of mobile traffic in Japan is around 71%; this rate for United states is estimated to be around 117% [1]. Also, the demand for bandwidth in wireless communications has been doubling every 18 months over the last 25 years [2]. As a result, larger bandwidths and tens of Gbps data rates will be required by 2020 [3,4].

Aside from the mobile applications, newer applications are being created that require higher data rates. For example, uncompressed high-definition TV (HDTV) has a bit rate of over 1.5 Gbps when transmitted from the DVD to the TV set. Ultrahigh definition TV (UHD) or 4k-TV has a 16 times increased resolution compared to HDTV. Therefore, data rates as high as 24 Gbps are required for their transmissions. For users in cities where the cost of optical cables is high and for the last mile problem, such as the last mile transmission of multiple channel HDTV, we need to have wireless data rates comparable to data rates in wireline communications [3]. In addition, Nano communication inside a computer [4], downloading high definition movies from a kiosk [5], transferring a large amount of data between mobile terminals and storage devices wirelessly also need higher wireless data rates.

One of the primary limitations in achieving high data rates is that the unlicensed bandwidth of microwave domain (300 MHz–100 GHz) is already reserved for some particular applications and only a limited bandwidth is available that can be used for communication purposes. As a result, advanced modulation and newer techniques (such as MIMO) have been developed to increase the spectral efficiency thus achieving higher data rates. However, based on Shannon's channel capacity formula there is an upper bound on the achievable data rate for a given bandwidth, and user demand has already exceeded this capacity in many cases [3]. One option is to use the Terahertz (THz) band [6,7]. The THz band extends from 100 GHz to 10 THz and as a result it has enormous available bandwidth that is not reserved for any specific application. Unfortunately THz signals are well absorbed by some molecules (specially water vapor molecules) in the atmosphere. Also, the signals are drastically attenuated on reflection. Therefore, THz applications may be limited to line of sight (LOS) and indoor scenarios [3]. In this paper we study the propagation behavior of

* Corresponding author.
E-mail addresses: moshir2@cs.pdx.edu (F. Moshir), singh@cs.pdx.edu (S. Singh).

http://dx.doi.org/10.1016/j.nancom.2016.07.008
1878-7789/

THz signals and subsequently examine the performance of various modulation schemes.

Two types of communication systems can be used in the THz domain. The first system uses continuous wave (CW) in which only a small portion of the bandwidth is used and the other system uses pulsed signals in which the entire band is used for communication. In the CW approach, the transmitter and receiver are tuned to a specific frequency that is less absorbed by atmospheric molecules and standard modulation methods are used. In the pulsed approach methods such as pulse position modulation have been studied using the very large bandwidth of the pulse. Our main contributions in this paper are:

- For the case of highly directional channels,
  - We present a pulse-modulation method in which the pulse is sliced into 2 GHz bands, each of which is independently modulated and the recreated pulse is transmitted. We show data rates of terabits/second can be achieved.
  - Since some bands are more prone to absorption than others, we describe an adaptive modulation scheme which uses knowledge of humidity to disregard certain bands when transmitting data.
- For the case of omni-directional antennas,
  - We study the performance of standard modulation methods when using three specific frequency bands that are more immune to absorption than other parts of the spectrum.
  - We then present rate-adaptation algorithms where the goal is to ensure fairness in channel access to different users, located at different distances from the access point.

The remainder of the paper is organized as follows. In the next section we summarize the related work in THz communications. In Section 3 we provide indoor THz channel characterization based on our measurements that is used in the Matlab simulations. In Section 4 we study pulsed signal modulation. Section 5 illustrates continuous wave modulation and our THz rate adaptation algorithms. Our conclusions are in Section 6.

2. Related work

Terahertz time-domain spectroscopy (THz-TDS) systems have been used in applications such as Terahertz imaging [8], biological spectroscopy [9], and communication in nano-networks [10]. However, to the best of our knowledge, the pulsed approach has not been used in Terahertz communication systems over a distance of longer than few millimeters, as in nano-networks. To date all communication systems have been highly directional continuous wave (CW) systems and mostly use simple modulation methods such as on–off keying (OOK) and Amplitude shift keying (ASK). For example, Song et al. [11] used 0.25 THz carrier frequency and transmitted 8 Gb/s error free data over 50 cm distance with ASK modulation. The bandwidth that they used was 4.5 GHz (4.5×10^{-3} THz).

Hirata et al. used 0.12 THz carrier frequency and were able to achieve 10 Gb/s data transmission rate with ASK modulation and forward error correction technique over a distance of 5.8 km [12]. Kallfass et al. [13] chose 0.22 THz carrier frequency with OOK modulation. The authors achieved data rates up to 40 Gb/s over a 50 cm distance. However, they only got low BER for data rates up to 15 Gbps while for higher data rates they were not able to get a good signal quality at the receiver. Zhang et al. [14] proposed a switch-based ASK modulator for an electronic based system. With this proposed method, the authors were able to achieve 10 Gb/s data rate with 0.135 THz carrier frequency over 20 cm distance.

Song et al. [15] considered data transmission on the 0.3 THz carrier frequency over a 50-cm distance. They achieved an error free data rate of as high as 24 Gb/s with ASK modulation. Besides ASK and OOK, duobinary baseband modulation has also being used for data transmission. Researchers in Bell Laboratories [16] used a higher carrier frequency of 0.625 THz and they achieved 2.5 Gb/s data rate over a distances less than 10 m.

Table 1
A summary of related works.

Frequency (THz)	Data rate (Gb/s)	Distance (m)	Modulation	Ref.
0.125	10	200	ASK	[23]
0.25	8	0.5	ASK	[11]
0.2	1	2.6	ASK	[24]
0.12	10	5800	ASK	[12]
0.3	0.096	0.7	64QAM	[25]
0.625	2.5	<10	Duobinary	[16]
0.22	15–40	10	OOK	[13]
0.24	25	60	OOK	[26]
0.0875	100	1.2	16QAM	[27]
0.135	10	0.2	ASK	[14]
0.3	24	0.5	ASK	[15]
0.146	1	0.025	OOK	[28]
0.22	30	20	ASK	[29]
0.542	2	0.01	ASK	[30]
0.14	10	1500	16QAM	[17]
0.24	30	40	8PSK	[31]
0.196	0.1	0.5	QPSK	[32]
0.34	3	0.3	16QAM	[18]
0.3	24	0.3	ASK	[33]
0.3	48	1	OOK	[34]
0.237	100	20	16QAM	[19]
0.4	40	2	ASK	[35]

Recently some researchers have utilized higher order modulation to achieve better spectrum efficiency. For example, Wang et al. [17] transmitted data over 1.5 km distance between transmitter and receiver. The authors achieved 10 Gb/s over a non-real-time channel with software modulator and 2 Gb/s over a real-time channel with hardware modulator using 16-quadrature amplitude modulation (16QAM). Lu et al. [18] demonstrated a system at 0.34 THz band. They used 16QAM modulation and transmitted 3 Gbps data over a 30 cm distance. Koenig et al. [19] for the first time achieved a data rate as high as 100 Gb/s over a 20 m distance between transmitter and receiver. The carrier frequency was 0.237 THz with a bandwidth of 0.035 THz. They utilized 8QAM and 16QAM modulation methods and designed relatively small opto-electronic based transmitter and electronic based receivers. Having small sizes, these transmitter and receiver systems may enable THz communication in future smartphones and tablets.

Considering THz channel attenuation, Han and Akyildiz [20] proposed a distance adaptive modulation method. In this method, based on transmitter–receiver distance, transmission windows with path loss of less than 160 dB are selected. These transmission windows are divided into smaller windows that are used to transmit multi-carrier signals. In this method, the assigned bandwidth and modulation order to each user depends on the transmitter–receiver distance. This method however suffers from the complexity of the control channel unit and channel feedback path. Also, the transmitter uses thousands of carriers to send data to a receiver. Having that many carriers at once requires a complex transmitter and receiver which is not feasible today. Han et al. [21] also proposed a multi-wideband distance-adaptive scheme that relies on pulse-based communications and does not support higher order modulations. In another scheme Han and Akyildiz [22] proposed a method that maximized the supported distance. This scheme requires a sophisticated control unit to calculate subwindows for each transmission link. This unit has to update the status of all links continuously due to changes in the channel. In this scheme the goal is to maximize the supported distance but the fairness among the users is not considered.

Table 1 is a summary of the work discussed above in addition to some other related work.

Please cite this article in press as: F. Moshir, S. Singh, Modulation and rate adaptation algorithms for terahertz channels, Nano Communication Networks (2016), http://dx.doi.org/10.1016/j.nancom.2016.07.008

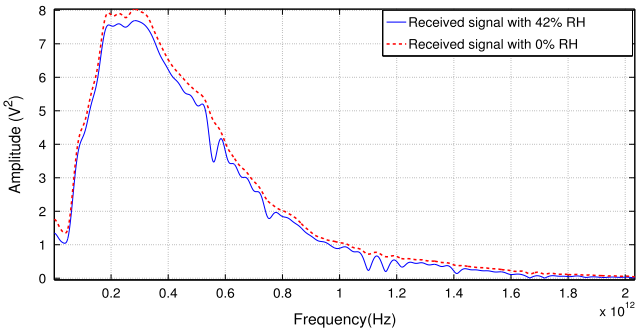

Fig. 1. Comparison of the frequency spectrum of the signals with 42% and 0% relative humidity (RH) with transmitter–receiver distance of 21.5 cm. The solid line corresponds to signal with 42% RH and the dotted line corresponds to the signal with 0% RH.

3. Channel model for simulations

In this section we characterize indoor THz channels and develop models that are used in simulation and analysis of directional and omni-directional THz communication systems. We first describe our testbed and then explain the channel measurements we conducted to develop our channel model. The data clearly shows significant attenuation due to absorption of some frequencies in the air. In Section 3.2 we develop a model for this attenuation. Our measurements were conducted using collimating lenses at both the transmitter and receiver.

3.1. Measurements

We use the commercially available Picometrix T-Ray 4000 system that is provided by Advanced Photonix, Inc (API) [36] in our measurements. Both the transmitter and receiver have a collimating lens. A collimating lens is a highly directional lens which produces parallel beams with the focus at infinity. We call the channel that has a collimating lens a *directional channel*. We set the initial transmitter–receiver distance to 11.5 cm and we go up to the transmitter–receiver distance of 66.5 cm with increments of 5 cm.

As the THz signal propagates through the channel, it is attenuated due to the resonance of some molecules in the atmosphere at specific frequencies. These resonance modes are due to rotational or vibrational transitions, that correspond to the THz frequency range. To explore the effect of water vapor, we conduct measurements in dry air and in humid air.

The humid air experiment has a relative humidity (RH) of 42%. For the dry case, we constructed a plastic tunnel around the transmitter and the receiver and blow dry air into the tunnel continuously to make sure that the RH remains at 0%. It should be noted that the temperature for all these measurements is set to 70 °F.

Fig. 1 shows the result of comparing the frequency spectrum of the signals with 0% and 42% RH from when transmitter–receiver distance is 21.5 cm. The figure shows that the detected THz energy is mainly below 2 THz in our system. Beyond 2 THz the signal is too weak to be distinguished from noise. Also, we see that in the received signal with 42% RH some frequencies are severely attenuated. These troughs correspond to the atmospheric attenuation that happens due to the presence of water vapor molecules in the air.

3.2. Modeling attenuation due to absorption

When the frequency of an electromagnetic signal reaches the resonant frequency of some molecule in the atmosphere, the molecule absorbs the signal's energy and changes its state between two quantum mechanical states. The absorption that occurs due to a transition between the two states is called an absorption line. The THz frequency spectrum is composed of many absorption lines that are unique for each gas molecule. For our channel model to be used in simulations, we need an accurate formula to compute this atmospheric frequency-specific attenuation.

Molecular absorption lines have a width and shape. The shape, Gaussian or Lorentzian distribution, is determined by the *broadening* mechanism and the intensity of a line is obtained by integrating the area under the absorption line and is proportional to the temperature and amount of the absorbing substance present in the environment. Using the radiative transfer theory [37] and given a set of parameters, absorption lines can be modeled at any temperature and pressure from HITRAN data base [38]. The following equations show how we can calculate absorption coefficient corresponding to each frequency [39]. The Lorentz half-width α is the weighted summation of air-broadened half-width, α_a^0, and self-broadened half-width α_s^0 for a specific molecule.

$$\alpha = [(1-q)\alpha_a^0 + q\alpha_s^0] \tag{1}$$

where, q is the mixing ratio of the absorber molecule in the air and is dimensionless. Then, we use the Van Vleck–Weisskopf (VVW) line shape to model the shape of the absorption lines. VVW line shape equation is as below [40]:

$$g(f) = \frac{1}{\pi}\left(\frac{f}{f_0}\right)^2 \left[\frac{\alpha}{\left(\frac{f}{c}-\frac{f_0}{c}\right)^2+\alpha^2} + \frac{\alpha}{\left(\frac{f}{c}+\frac{f_0}{c}\right)^2+\alpha^2}\right]. \tag{2}$$

Here, c is the propagation speed, f_0 is the frequency of the line center, and f is the frequency for which the absorption is calculated.

Using the Beer–Lambert law, the absorption spectrum for the particular molecule is found to be quantitatively related to the presented amount of material. The following equation shows how to calculate the absorption coefficient, $\kappa(f)$, of the absorber corresponding to a line:

$$\kappa(f) = uSg(f). \tag{3}$$

Here, S is the line strength ($\mathrm{cm}^{-1}/(\mathrm{mol/cm}^2)$), and u is the absorber thickness that is the mole number of the absorber in one cm^3 of environment. Sum of the absorption due to each line, l, gives the total absorption coefficient at any frequency.

$$K(f) = \sum_l \kappa_l(f). \tag{4}$$

In our experiment, we consider absorption lines up to 2 THz for water vapor (H_2O), oxygen (O_2), nitrogen (N_2), and carbon dioxide (CO_2).

We calculate the total absorption coefficient for different humidity levels. Fig. 2 shows the result in dB/cm for the range of 0–2 THz for 0%, 10%, 40%, and 80% RH levels. As the figure shows and we expected, with higher humidity the attenuation coefficient is increased. The attenuation coefficient corresponding to some frequency bands is slightly attenuated with the increase of humidity, whereas other frequencies are drastically attenuated. The result is in a good agreement with other works [41,42].

3.3. Directional channel model

In the past few years the THz channel model has been derived for multiple scenarios [43–47]. In our paper we consider line-of-sight channel where there is no multi path.

Please cite this article in press as: F. Moshir, S. Singh, Modulation and rate adaptation algorithms for terahertz channels, Nano Communication Networks (2016), http://dx.doi.org/10.1016/j.nancom.2016.07.008

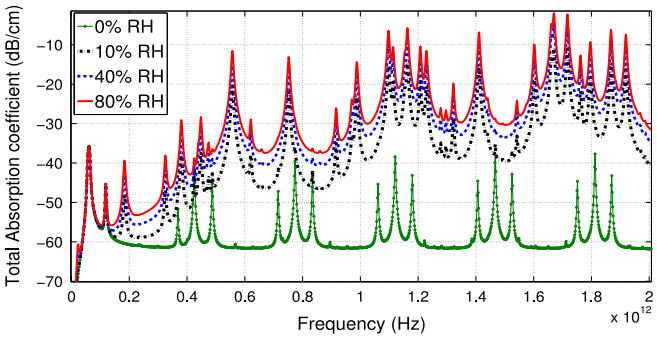

Fig. 2. Atmospheric attenuation coefficient for different relative humidity (RH) levels.

We saw that the primary impairment to THz communications is the absorption of the transmitted signal by water vapor molecules in the channel. According to Beer–Lambert law transmittance of the signal decreases exponentially with the transmitter–receiver distance [48]. Therefore, the transfer function of the channel is set to:

$$H(f) = e^{-(j2\pi f\tau + dK(f))} \tag{5}$$

where, d is the transmitter–receiver distance, τ is the propagation delay in seconds through distance d, and $K(f)$ is the atmospheric attenuation from (4). In the equation there is no free-space propagation loss because we are only considering short-range channels formed by collimating lenses which result in a parallel beam.

Having the transfer function from (5), we can characterize the directional channel as below:

$$R(f) = S(f)H(f) + Noise. \tag{6}$$

Eq. (6) shows the effect of the channel on the signal. The input signal, $S(f)$, is multiplied by the transfer function, $H(f)$, and *Noise* is added to the result and $R(f)$ that is the signal in frequency domain is received at the receiver. For *Noise*, we use a standard model and assume it is a random variable with a Gaussian distribution with mean power of −174 dBm/Hz. Based on the channel model from (6), we can find the received signal for a specific humidity and transmitter–receiver distance.

Fig. 3 compares experimental measurements with our simulation results for a 51.5 cm transmitter–receiver distance with 0% RH and 42% RH. Simulation results, shown as a solid line, are calculated from our model given above and the experimental results are illustrated by the dotted line. As can be observed from this figure, the measurement results are in close agreement with values calculated from our proposed model, especially at high frequencies.

3.4. Omni-directional channel model

To characterize the THz omni-directional channel we find the total attenuation coefficient $K(f)$ from (4). As we discussed earlier, according to Beer–Lambert law the transmittance of the signal decreases exponentially with transmitter–receiver distance. Also, based on Friis equation, in the case of omni-directional antennas, the signal also suffers the effect of free space path loss. Therefore, the transfer function for our channel is as follows.

$$H(f) = \frac{\lambda}{4\pi d} \times e^{-(i2\pi f\tau + dK(f))}. \tag{7}$$

In this equation, λ is the wavelength in cm for which the transfer function is calculated, d is the transmitter–receiver distance in cm, and τ is the time in seconds required for the signal to travel through distance d.

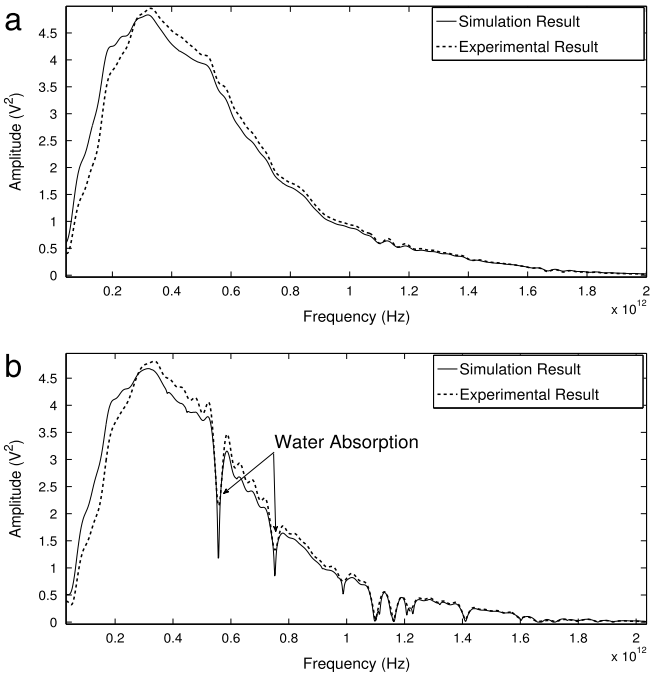

Fig. 3. Simulated vs. Experimental signal over 50 cm distance and (a) 0% RH and (b) 42% RH. Solid and dotted line represent simulation and experimental results, respectively.

4. Pulsed signal modulation

In this section we use simulations to study pulsed modulation using the channel model derived above in Section 3.3. The work reported in this chapter assumes the presence of collimating lenses at the transmitter and receiver giving us a highly directional channel. We first use the concept of frequency domain differential phase shift keying (FD-DPSK) modulation in which each pulse corresponds to many data symbols. Then we propose an adaptive algorithm to improve the bit error rate (BER). We also discuss the use of multiple transmitters and multiple receivers with FD-DPSK modulation to linearly increase throughput. Then we employ amplitude shift keying (ASK) modulation where each pulse corresponds to only one data symbol.

4.1. FD-DPSK modulation

We initially use frequency domain differential phase shift keying (FD-DPSK) modulation originally proposed by Rhee et al. [49]. In this method, the data is modulated based on the phase difference between adjacent spectral bands of the signal. The receiver retrieves the modulated data by means of wavelength shift with an interferogram.

For modulating the spectral domain of the pulsed signal, we assume an acousto-optic modulator (AOM) pulse shaper technique [50,49]. In our system, the transmitter consists of a femtosecond pulse laser and a sequence of grating → lens → AOM → lens → grating. The AOM of our system has a 40 mm aperture size with 1000 pixel spectral resolution. It takes ∼10 μs for the input radio frequency (RF), which has the carrier frequency of 200 MHz and modulation bandwidth of 100 MHz, to propagate through the AOM. Meanwhile, the grating and lens slice the femtosecond pulse into 1000 bands. Since the bandwidth of our signal is 2 THz, each of these frequency bands is 2 GHz wide. The sliced pulse is then passed through the AOM and phase modulated with the phase information of the modulating RF signal. As is clear from Fourier transform relations, this output pulse spreads in time

Please cite this article in press as: F. Moshir, S. Singh, Modulation and rate adaptation algorithms for terahertz channels, Nano Communication Networks (2016), http://dx.doi.org/10.1016/j.nancom.2016.07.008

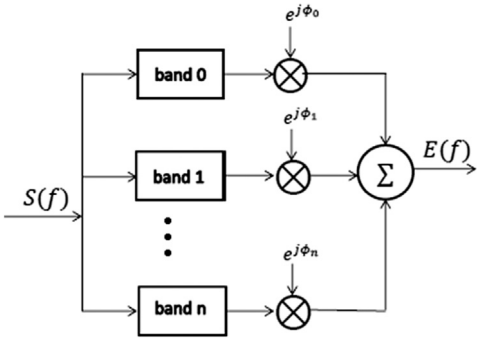

Fig. 4. Transmitter block diagram.

and takes the time window equal to one of the spectral bands, which is 1 ns.

We use FD-D*M*PSK modulation [49], where M is the modulation order. Since we are using differential phase modulation methods, for sending n symbols, $a_i \in \{1, 2, \ldots, n\}$, the transmitter needs to send an extra symbol as the reference phase. Therefore, the spectrum of the pulse signal is sliced into $n+1$ bands.

The modulation process is as follows: consider n symbols $a_1, a_2, a_3, \ldots, a_n$, where $a_i \in \{1, 2, \ldots, M\}$ and $1, 2, \ldots, M$ correspond to symbols corresponding to bit sequences such that the Hamming distance between each two adjacent symbols is 1.

First, the phase function, $\psi(a_i)$, for each of these symbols is set as follows:

$$\psi(a_i) = \frac{(a_i - 1)\pi}{2^b - 1}, \quad \text{for } i = 1, \ldots, n. \tag{8}$$

Then, the corresponding $n+1$ phases are found:

$$\phi_i = \begin{cases} 0 & \text{for } i = 0, \\ \psi(a_i) + \phi_{i-1}, & \text{for } i = 1, 2, \ldots, n \end{cases} \tag{9}$$

where ϕ_0 corresponds to the reference phase.

Fig. 4 shows the transmitter block diagram. We generate the femtosecond pulse as a step rectangular pulse function that corresponds to a sinc function with bandwidth of 2 THz in the frequency domain. We slice the frequency domain of the signal into $n+1$ bands and then each band is modulated with the phase obtained from (9) as below.

$$E(f) = \sum_{i=0}^{n} e^{j\phi_i} S(f - f_i, \delta f). \tag{10}$$

Here, $E(f)$ is the spectral complex value of the femtosecond signal and $S(f - f_i, \delta f)$ is the spectral value of ith band. Note that $f_i = f_0 + i\delta f$ is the central frequency, and $\delta f = \Delta f/(n+1)$ is the bandwidth of the ith band. Here, f_0 is the central frequency of the first spectral band and $\Delta f = 2$ THz. The modulated signal is then passed through the channel and is changed based on the channel model.

$$R(f) = E(f)H(f) + Noise \tag{11}$$

where, $H(f)$ is the transfer function of the directional channel from (5), *Noise* is the noise in the channel that is added to the signal, and $R(f)$ is the received signal at the receiver.

At the receiver, the signal is first divided by the transfer function of the channel, $H(f)$, to decrease the effect of channel impairments. Fig. 5 shows the receiver block diagram. As can be seen from the figure, the received signal, $R(f)$, is first passed through a filter and is sliced into $n+1$ bands. A copy of the signal is shifted in frequency by δf. Thus, the shifted $(i-1)$th band has the central frequency of the

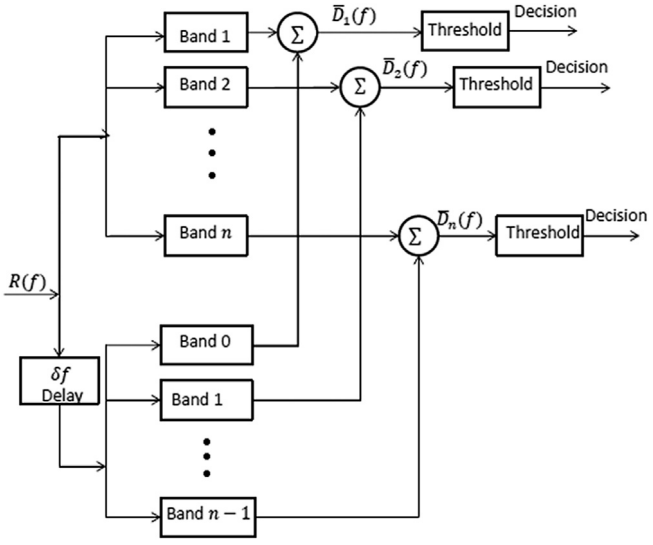

Fig. 5. Receiver block diagram.

unshifted ith band. Combining the ith band of the unshifted signal with the $(i-1)$th band in the shifted signal we get the following.

$$\bar{D}_i(f) = \frac{1}{2}[\acute{R}(f - f_{i-1}, \delta f) + R(f - f_i, \delta f)], \quad \text{for } i = 1, \ldots, n. \tag{12}$$

In (12), $R(f - f_i, \delta f)$ is the ith band of the received signal, and $\acute{R}(f - f_i, \delta f)$ is the ith band of the received signal that is shifted by δf.

We now compare the intensity of the $\bar{D}_i(f)$, $|\bar{D}_i(f)|^2$, with different thresholds at the receiver that are found based on the following equations.

$$\bar{E}_i(f) = \frac{1}{2}(e^{j\phi_{i-1}} S(f - f_{i-1}, \delta f) + e^{j\phi_i} S(f - f_i, \delta f)) \quad \text{for } i = 1, \ldots, n \tag{13}$$

$$|\bar{E}_i(f)|^2 = \frac{1}{2}|\bar{S}_i(f)|^2 \times |1 + e^{2j\psi(a_i)} + 2e^{j\psi(a_i)}| \quad \text{for } i = 1, \ldots, n. \tag{14}$$

Here, $\bar{S}_i(f)$ is the average of each two consecutive unmodulated spectral bands and is found as follows.

$$\bar{S}_i(f) = \frac{1}{2}[S(f - f_{i-1}, \delta f) + S(f - f_i, \delta f)], \quad \text{for } i = 1, \ldots, n. \tag{15}$$

For n symbols we get $(n-1)$ thresholds.

$$th_i^{j-1} = \frac{|\bar{E}_i(f)|^2_{a_{j-1}} + |\bar{E}_i(f)|^2_{a_j}}{2}, \quad \text{for } j = 2, \ldots, n. \tag{16}$$

Having the thresholds, the received symbols are detected. Where, r_i is the ith detected symbol in the receiver.

$$r_i = \begin{cases} a_1, & \text{if } |\bar{D}_i(f)|^2 \geq th_i^1 \\ a_2, & \text{else if } |\bar{D}_i(f)|^2 \geq th_i^2 \\ \vdots & \\ a_{n-1}, & \text{else if } |\bar{D}_i(f)|^2 \geq th_i^{n-1} \\ a_n, & \text{otherwise.} \end{cases} \tag{17}$$

Simulation results for FD-DMPSK. We use Matlab for our simulation and utilize five different modulation schemes: FD-DBPSK, FD-DQPSK, FD-D8PSK, FD-D16PSK, and FD-D64PSK. For each of these

Please cite this article in press as: F. Moshir, S. Singh, Modulation and rate adaptation algorithms for terahertz channels, Nano Communication Networks (2016), http://dx.doi.org/10.1016/j.nancom.2016.07.008

Table 2
The list of figures that show BER vs. E_b/N_0 for different modulation schemes corresponding to transmitter–receiver (Tx–Rx) distances of 50 and 100 cm.

Tx–Rx distance (cm)	RH		
	0%	40%	80%
50	Fig. 6	Fig. 7	Fig. 8
100	Fig. 9	Fig. 10	Fig. 11

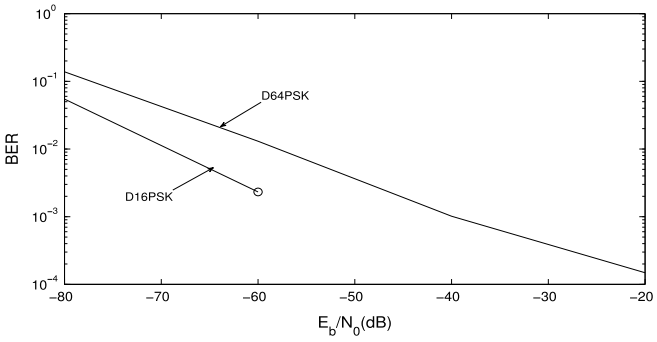

Fig. 6. BER vs. E_b/N_0 for 0% RH and transmitter–receiver distance of 50 cm.

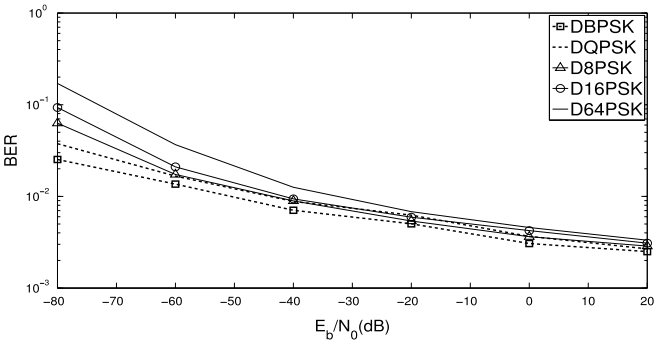

Fig. 7. BER vs. E_b/N_0 for 40% RH and transmitter–receiver distance of 50 cm.

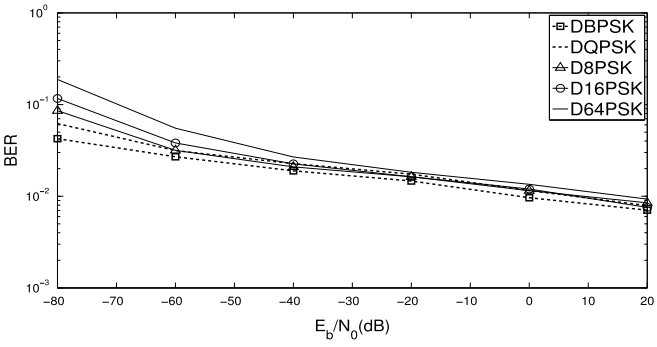

Fig. 8. BER vs. E_b/N_0 for 80% RH and transmitter–receiver distance of 50 cm.

modulations, we consider 50 cm and 100 cm distances between transmitter and receiver. Each case is simulated for different RH levels of 0%, 40%, and 80%. Table 2 lists the figures that show BER vs. E_b/N_0 for different modulation schemes. In these figures, we ignore the cases with BER $< 10^{-6}$. In Figs. 6 and 9, when the relative humidity is 0% and $E_b/N_0 > -80$ dB, the BER corresponding to FD-DBPSK, FD-DQPSK, and FD-D8PSK, is equal to 0. It is interesting to note that the BER curves for all modulation schemes are close to one another.

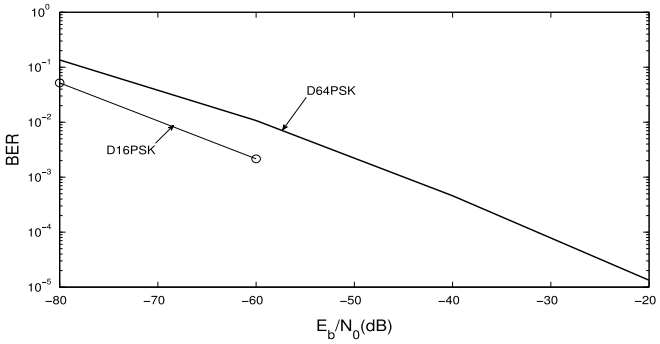

Fig. 9. BER vs. E_b/N_0 for 0% RH and transmitter–receiver distance of 100 cm.

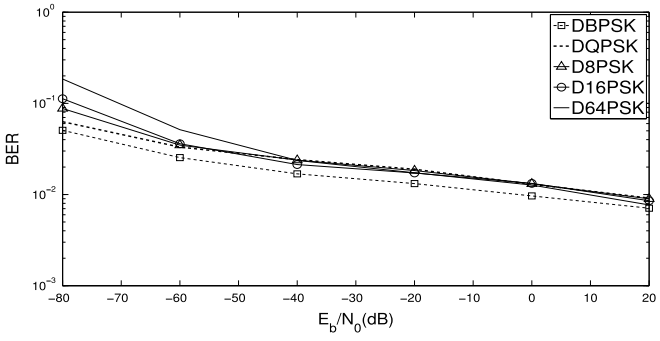

Fig. 10. BER vs. E_b/N_0 for 40% RH and transmitter–receiver distance of 100 cm.

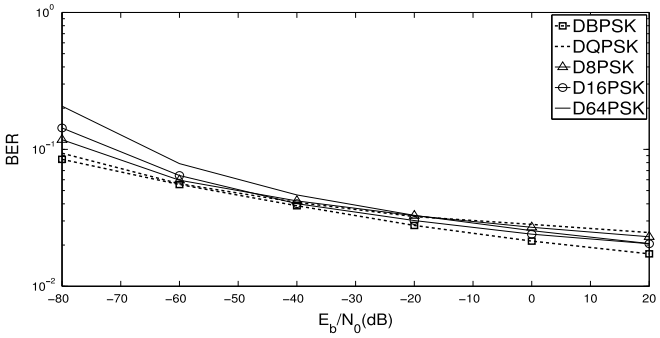

Fig. 11. BER vs. E_b/N_0 for 80% RH and transmitter–receiver distance of 100 cm.

4.1.1. *Adaptive FD-DPSK modulation*

As atmospheric attenuation depends on frequency, some bands are attenuated drastically. In adaptive FD-DPSK we exclude these bands from the modulation. The set of bands that are excluded depends on the transmitter–receiver distance as well as the humidity level. Thus, at lower humidity or smaller distances, fewer bands are excluded, since the attenuation is not significant. While this adaptive method decreases the number of symbols that are sent, it enhances the BER for the E_b/N_0. Fig. 12 shows the error rate for each band and the corresponding humidity absorption coefficient when the $E_b/N_0 = 0$ dB, transmitter–receiver distance is 100 cm, and the relative humidity is 80%. As is shown in the figure, all of the bands that cause errors have center frequency higher than 1 THz. The reason is that the sync signal in our simulation has more power for frequencies below 1 THz and even though it is attenuated, the corresponding bands are detectable at the receiver. On the other hand, the sync signal has less power for the bands with center frequency of higher than 1 THz. Hence, the attenuation will cause errors in these bands.

Please cite this article in press as: F. Moshir, S. Singh, Modulation and rate adaptation algorithms for terahertz channels, Nano Communication Networks (2016), http://dx.doi.org/10.1016/j.nancom.2016.07.008

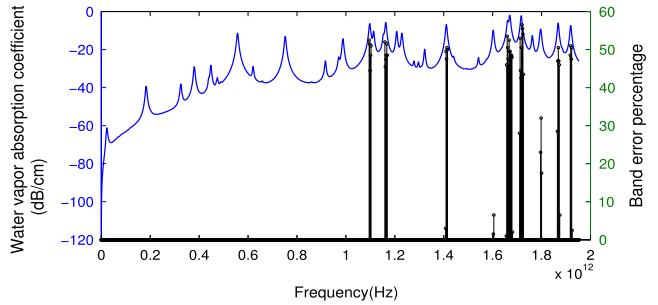

Fig. 12. Band error rate vs. water vapor absorption coefficient for $E_b/N_0 = 0$ dB, transmitter–receiver distance = 100 cm, and RH = 80%.

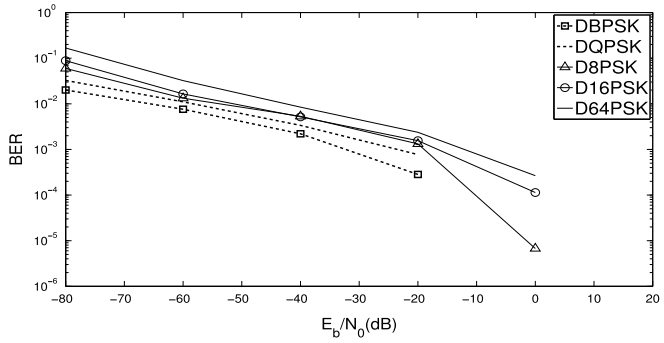

Fig. 13. BER vs. E_b/N_0 corresponding adaptive modulation schemes for 40% RH and transmitter–receiver distance of 50 cm.

We exclude the *erroneous bands* from the modulation based on the following algorithm.

Adaptive FD-DPSK Modulation Algorithm

1: Categorize the available bands into two groups:
   - *error-free bands*: bands that will carry useful information
   - *erroneous bands*: bands that should be excluded from the modulation
2: At the transmitter: find the phase corresponding to *error-free bands* from (9)
3: Set the phase corresponding to *erroneous bands* to 0
4: Use the RF signal, which is the superposition of phases found in steps 1 and 2, to modulate the pulse
5: At the receiver: Ignore the *erroneous bands* and use the remaining bands to decode the received data

Simulation results for adaptive FD-M DPSK modulation. In adaptive FD-DPSK, we find the *erroneous bands* for $E_b/N_0 = 0$ that have BER $\geq 10^{-2}$. Table 3 shows the number of *erroneous bands* for different scenarios.

Figs. 13 and 14 compare BER vs. E_b/N_0 of adaptive modulation schemes when transmitter–receiver distance is 50 cm and the RH is 40% and 80%, respectively.

Figs. 15 and 16 compare BER vs. E_b/N_0 of modulation schemes when transmitter–receiver distance is 100 cm and RH is 40% and 80%, respectively.

As is obvious from the figures, the BER has decreased significantly using adaptive modulation schemes in comparison with the regular modulation schemes. For example, at $E_b/N_0 = 20$ dB, with 50 cm transmitter–receiver distance and 80% RH, BER $\sim 10^{-2}$ has been reduced to $\sim 10^{-4}$ in FD-D64PSK, to $\sim 10^{-5}$ in FD-D16PSK, and 0 for FD-D8PSK, FD-DQPSK, and FD-DBPSK.

Table 3
Number of *erroneous bands* with $E_b/N_0 = 0$ and BER $\geq 10^{-2}$ for FD-DPSK scheme and transmitter–receiver (Tx–Rx) distances of 50 and 100 cm.

Tx–Rx distance (cm)	RH	
	40%	80%
50	9	29
100	30	55

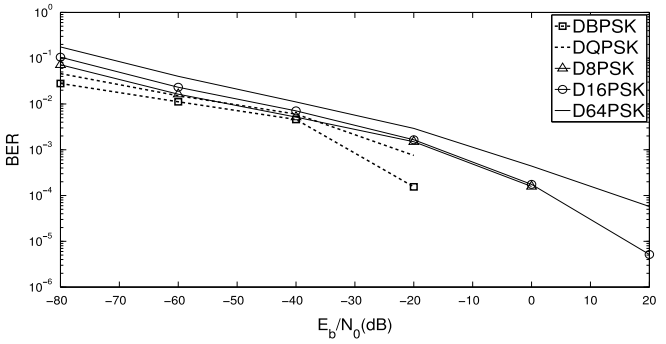

Fig. 14. BER vs. E_b/N_0 corresponding adaptive modulation schemes for 80% RH and transmitter–receiver distance of 50 cm.

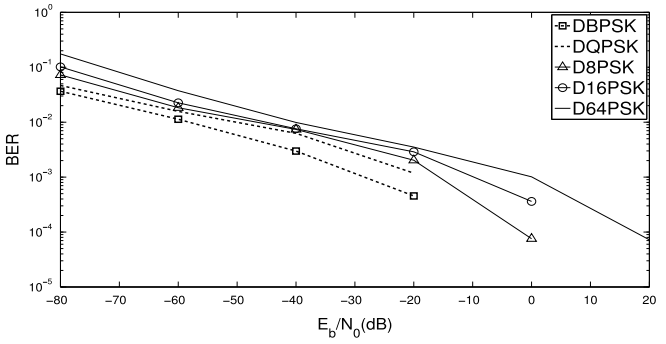

Fig. 15. BER vs. E_b/N_0 corresponding adaptive modulation schemes for 40% RH and transmitter–receiver distance of 100 cm.

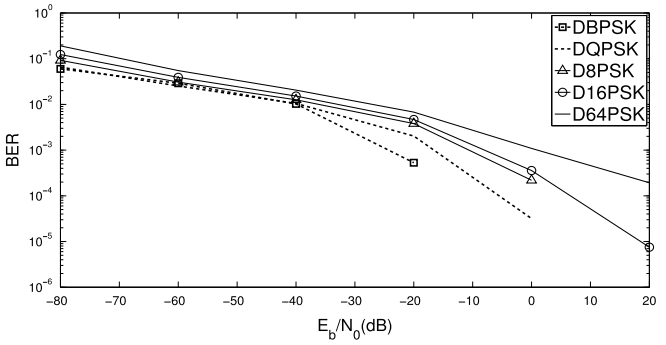

Fig. 16. BER vs. E_b/N_0 corresponding adaptive modulation schemes for 80% RH and transmitter–receiver distance of 100 cm.

4.2. Multiple transmitters and achievable data rates based on adaptive FD-DPSK modulation

As explained earlier in Section 4.1, based on the AOM structure and its aperture size, the transmitter sends a pulse every 10 μs that takes 1 ns. Therefore, up to 10 000 transmitters can be incorporated in a time division multiplexing (TDM) system to achieve higher data rates. Fig. 17 shows how this idea works. Having multiple transmitters, Table 4 shows the aggregate number of error-free detected bits at the receiver, when $E_b/N_0 = 0$ dB.

Please cite this article in press as: F. Moshir, S. Singh, Modulation and rate adaptation algorithms for terahertz channels, Nano Communication Networks (2016), http://dx.doi.org/10.1016/j.nancom.2016.07.008

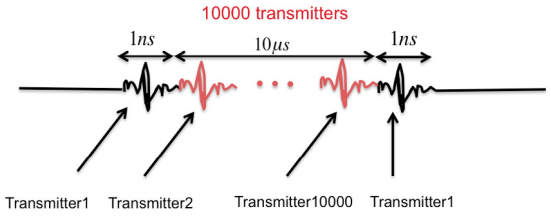

Fig. 17. Up to 10,000 transmitters can generate pulses in a TDM system and achieve higher data rates.

Table 4
Adaptive FD-DPSK bit rate for multiple scenarios with $E_b/N_0 = 10$ dB.

	RH	Distance	
		50 (cm)	100 (cm)
DBPSK	0%	0.999 Tb/s	0.999 Tb/s
	40%	0.999 Tb/s	0.999 Tb/s
	80%	0.999 Tb/s	0.999 Tb/s
DQPSK	0%	1.998 Tb/s	1.998 Tb/s
	40%	1.998 Tb/s	1.998 Tb/s
	80%	1.998 Tb/s	1.998 Tb/s
D8PSK	0%	2.997 Tb/s	2.997 Tb/s
	40%	2.997 Tb/s	2.997 Tb/s
	80%	2.997 Tb/s	2.997 Tb/s
D16PSK	0%	3.996 Tb/s	3.996 Tb/s
	40%	3.996 Tb/s	3.996 Tb/s
	80%	3.9956 Tb/s	3.995 Tb/s
D64PSK	0%	5.994 Tb/s	5.994 Tb/s
	40%	5.994 Tb/s	5.9907 Tb/s
	80%	5.9925 Tb/s	5.9906 Tb/s

One important issue that needs to be addressed is the possibility of inter-symbol interference caused by temporal broadening of the consecutive 1 ns pulses. Temporal broadening may caused by the frequency-selective nature of the channel. For instance, if different frequencies propagate at different speeds in the media (due to different refractive indices) and suffer different attenuation, the received pulse will experience broadening. However, as shown in [51] the refractive index is unchanged to the fifth decimal place for the frequencies we studied. Furthermore, [52] shows terahertz pulses are stable for long distances and we only begin seeing overlapping pulses (i.e., the transmitted pulse begins showing effects of broadening) at distance of 2 km. For the short distances we study in this paper, we therefore will see little or no ISI between consecutive pulses.

4.3. Multiple users in FD-DPSK modulation

When we use the FD-DQPSK scheme, since we are splitting the 2 THz bandwidth into 2 GHz bands, the reconstituted pulse spreads in time and is now 1 ns long. Note that the AOM takes 10 μs to set to the next symbol. Therefore, by using 10,000 AOMs staggered in time with respect to each other by 1 ns, we can fully occupy the channel as shown in Fig. 18. In the figure we illustrate the 1000, 2 GHz channels and consecutive AOMs used to generate the modulated pulse. Using this simple scheme, we can achieve aggregate data rates of 1.98 Tb/s and 1.94 Tb/s when the transmitter–receiver distance is 50 cm and the relative humidity is 40% and 80%, respectively. The figure also illustrates how we can use this channel structure to support multiple simultaneous users. In the figure we show that user 1 is allocated 3 slots, where a slot is a combination of frequency band and AOM. If we assume that user 1 only gets 3 slots every 10 μs the data rate it can achieve is 400 kbps. This is because one of the slots serves as the reference phase while the other two are each carrying 2 bits of data. It is easy to see that this structure will allow an access point to multiplex data streams for many users in a very flexible way.

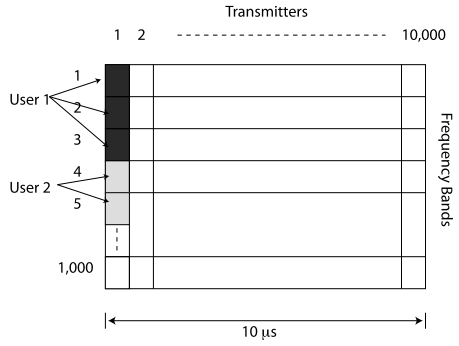

Fig. 18. Using multiple transmitters.

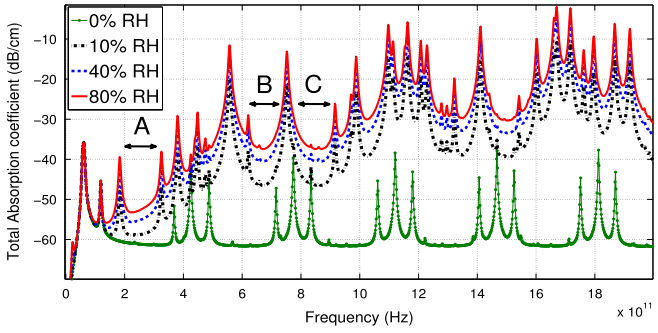

Fig. 19. Atmospheric attenuation coefficient for multiple relative humidity levels and the three channels with relatively less attenuations.

Finally, we need to discuss the question of how a receiver can determine its slot allocation as well as which of the bands is not being used (due to the weakness of the signal caused by humidity and distance). A possible solution is to use designated lower frequency bands (below 300 GHz) for sending control information at some periodicity since these bands are relatively immune to water absorption. Therefore, in our proposed approach, the transmitter first estimates the relative humidity and uses some form of ranging to determine the distance at which each receiver is located. It then estimates which bands should not be used for each user, performs an allocation of slots and transmits this information in the control slots. Interestingly, some slots may be usable for nearby users and not for distant users. This gives us more choices in determining slot allocation.

5. Continuous wave modulation and rate adaptation

In this section we study omni-directional terahertz channels. Unlike the analysis in the previous section we assume a continuous wave (CW) system rather than a pulsed system. Continuous waves have smaller bandwidth than pulsed signals that we use in directional channels. The THz transmitter and receiver are tuned to a specific frequency that is not attenuated drastically by water vapor molecules.

Fig. 19 shows atmospheric attenuation coefficient in dB/cm as a function of frequency for the range of 0–2 THz for 0%, 10%, 40%, and 80% RH levels. The result shows that there are three windows A, B, and C in which the absorption coefficient is smaller compared to the other frequency bands. Hence, we use the center carrier frequencies of 237.5 GHz (channel A), 677.5 GHz (channel B) and 872.5 GHz (channel C) with the bandwidth of 35 GHz in this study. Fig. 20 plots the calculated received power based on the transfer function from (7) for these three channels. As we expected, for channel C that has the highest center frequency the calculated received power is lower than the other channels.

Please cite this article in press as: F. Moshir, S. Singh, Modulation and rate adaptation algorithms for terahertz channels, Nano Communication Networks (2016), http://dx.doi.org/10.1016/j.nancom.2016.07.008

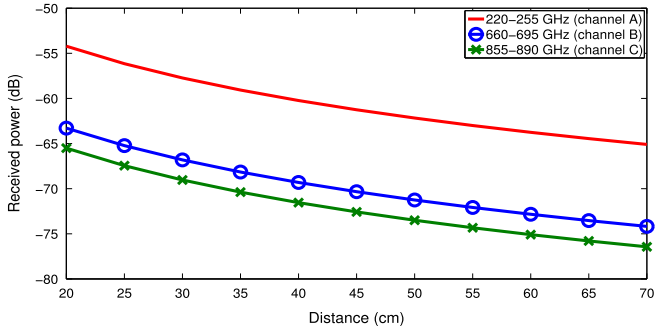

Fig. 20. Received power of 220–255 GHz (channel A), 660–695 GHz (channel B) and 855–890 GHz (channel C) using omni-directional antennas.

5.1. Rate adaptation algorithms

In order to explain the overall problem addressed in this section, it is useful to first present the system model. Assume the presence of a terahertz access point (TAP) located in the ceiling so that it has line of sight (LOS) to all the potential users. Let us also assume that there is a WiFi link between the users and the TAP. The WiFi link is used as the control channel for the terahertz downlink. Thus, the WiFi link is used in the normal way to register users into the network and to access the Internet. The only difference is that when sending large amounts of data to the user, the TAP sends the data stream over the terahertz channel rather than the WiFi link.

We develop two rate adaptation algorithms in which TAP adapts the modulation order based on the channel parameters. In the first algorithm we use a single channel (A, B, or C) only. Later, in Section 5.1.2, we develop a second algorithm that utilizes all three channels (A, B, and C) together. We assume that the WiFi channel is used to estimate the distance to each user and the TAP also measures the relative humidity of the air. Using this information, the TAP can compute the expected E_b/N_0 for different users and different modulation schemes. Then it selects the highest order modulation with BER $\leq$ BER_{Th}, where BER_{Th} is the maximum BER (bit error rate) that can be tolerated at each receiver. We use MPSK (phase shift keying) modulation in which M is changed based on the user distance from the TAP.

Our first algorithm is called single channel algorithm (SCA) in which TAP uses a single channel to send data to the users, whereas in the multiple channel algorithm (MCA) TAP uses three channels A, B, and C at the same time to increase the data rate of the system.

5.1.1. Single Channel Algorithm (SCA)

To have a fair connection in which all users can achieve similar data rates, TAP sends data to each user in a time division multiplexing (TDM) system. For that, TAP assigns the smallest time slot, $T_{\min}$, to the user that has the highest order modulation. For users with lower order modulation, TAP selects multiples of $T_{\min}$ such that all users receive almost the same data rate.

Imagine that there are 4 users and based on their distances to TAP, $d_1, \ldots, d_4$, the received E_b/N_0 for each of them is such that the TAP assigns 16PSK, 8PSK, QPSK, and BPSK modulation to the users, respectively. Fig. 21 is a schematic of this system and Fig. 22 shows how TAP assigns time slots to each user in order to maintain fairness in the channel.

In general, the ith user in its time slot receives the upper bound of b_i bits of error free information that is equal to the following equation.

$$b_i = \left\lfloor \frac{T_i}{T_s} \right\rfloor \log_2 M_i - \left[\text{BER} \times \left\lfloor \frac{T_i}{T_s} \right\rfloor \log_2 M_i \right]. \quad (18)$$

Here, T_s is the symbol time, T_i is the time slot, and M_i is the modulation order that are assigned to the ith user. Therefore,

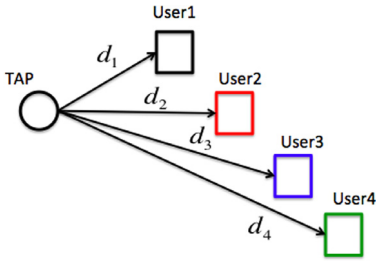

Fig. 21. System schematic.

Fig. 22. Time slots assigned to each user in SCA.

having the total of I users, we can calculate the data rate for each user, r_i, as follows.

$$r_i = \frac{b_i}{\sum_{i=1}^{I} T_i}. \quad (19)$$

5.1.2. Multiple Channel Algorithm (MCA)

In this algorithm, TAP uses channels A, B, and C simultaneously to send data to users and achieve higher data rate for each user. As we will see later in Section 5.2, each channel covers different ranges of TAP-user distances. The reason is that the frequency of channel A is lower than the other two channels and the lower frequency means longer wavelengths. Also, from (7), we saw that signal with shorter wavelengths attenuated more. Therefore, using channel A, TAP can send data to users with longer distances in comparison with channels B and C. For the same reason channel B covers users with longer distance than channel C.

In MCA, time slots with the same duration T are assigned to all users. In each time slot, TAP sends data to three users using different channels such that fairness is maintained among users and the highest data rate is achieved. The following is the rate adaptation algorithm that is used in MCA.

Multiple Channel Algorithm (MCA)

1: Assign $Counter = 0$ to all users
2: $Range_A$: The longest distance that can be covered using channel A
3: $Range_B$: The longest distance that can be covered using channel B
4: $Range_C$: The longest distance that can be covered using channel C
5: **for** each *timeSlot* **do**
6: $minCounter_A$=Min($Counter$) of users with distances$\leq$ $Range_A$
7: Find the user with the longest distance that has $Counter = minCounter_A$, assign channel A to the user
8: If a user is found, find the highest order modulation method using channel A that has BER$\leq$$BER_{Th}$ and
9: Add the $log_2 M$ corresponding to the selected modulation to the user's $Counter$
10: $minCounter_B$=Min($Counter$) of users with distances$\leq$ $Range_B$
11: Find the user with the shortest distance that is in ($Range_C$, $Range_B$] and has $Counter = minCounter_B$, assign channel B to the user

Please cite this article in press as: F. Moshir, S. Singh, Modulation and rate adaptation algorithms for terahertz channels, Nano Communication Networks (2016), http://dx.doi.org/10.1016/j.nancom.2016.07.008

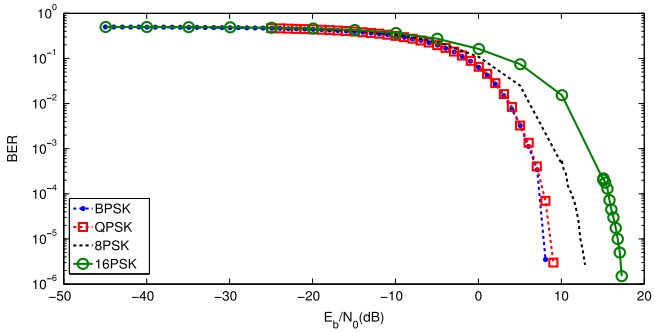

Fig. 23. Bit error rate (BER) vs. received E_b/N_0 for modulation methods.

12: If did not find such user, find the user with the longest distance$\leq$ $Range_C$ that has $Counter = minCounter_B$, assign channel B to the user
13: If a user is found, find the highest order modulation method using channel B that has BER$\leq$BER$_{Th}$ and
14: Add the $log_2 M$ corresponding to the selected modulation to the user's *Counter*
15: $minCounter_C$=Min(*Counter*) of users with distances$\leq$ $Range_C$
16: Find the user with the shortest distance that has $Counter = minCounter_C$, assign channel C to the user
17: If a user is found, find the highest order modulation method using channel C with BER$\leq$BER$_{Th}$ and
18: Add the $log_2 M$ corresponding to the selected modulation to the user's *Counter*
19: **end for**

MCA keeps track of the downlink data rate that is assigned to each user with the *Counter* variable. The upper bound of the received data bits for the ith user is equal to the following equation.

$$b_i = \sum_{t=1}^{K} \sum_{z=1}^{3} \left(\left\lfloor \frac{T}{T_s} \right\rfloor \log_2 M_{iz} - \left[\mathrm{BER}_{iz} \times \left\lfloor \frac{T}{T_s} \right\rfloor \log_2 M_{iz} \right] \right). \quad (20)$$

Here, T is the duration of each time slot, K is the number of time slots, M_{iz} is the modulation order and BER_{iz} is the bit error rate for the ith user that is receiving data on channel z, where $z = 1$, $z = 2$, and $z = 3$ correspond to channels A, B, and C, respectively. Therefore, the data rate for user i is found as follows.

$$r_i = \frac{b_i}{\sum_{t=1}^{K} T}. \quad (21)$$

5.2. Simulation results

We use Matlab for the simulation. The symbol rate of our system is set to 25 GBd/s and we use the raised cosine filter with rolloff factor 0.4. Fig. 23 shows BER corresponding to all modulation methods for received E_b/N_0 (dB) levels.

We set the BER_{Th} to 10^{-4} and we select the highest order modulation that has BER $<$ BER_{Th} for the received E_b/N_0. Based on the channel model from (7) and the transmitter power of 35 mW, we calculate the received E_b/N_0 and the corresponding BER for TAP-user distances of 100–2000 cm for channels A, B, and C. Figs. 24–26 show BER vs. distance for the modulation methods when we use channel A, B, or C, respectively. We should note that BER less than 10^{-6} is not shown in the figures.

As the figures show, the received power is attenuated more when we use higher frequencies. Therefore, channel A gives the best result, whereas channels B and C have higher BER for the same TAP-user distance. Having the BER vs. distance corresponding to each channel, we calculate data rate vs. distance. Figs. 27–29 show the result when TAP uses channel A, B, or C, respectively.

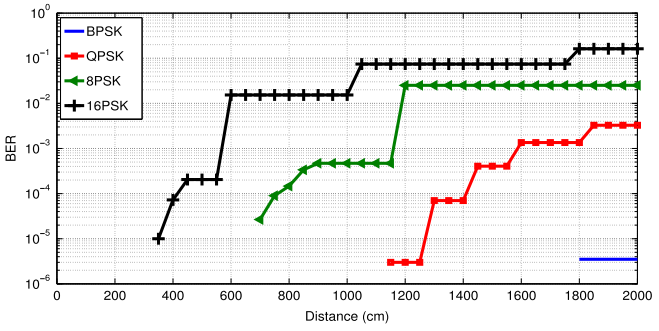

Fig. 24. Bit error rate vs. distance (cm) for modulation methods using channel A for transmission.

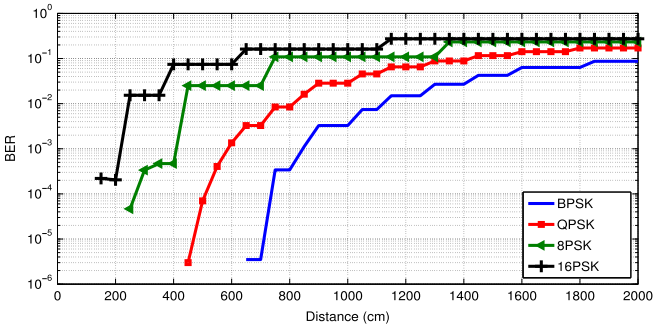

Fig. 25. Bit error rate vs. distance (cm) for modulation methods using channel B for transmission.

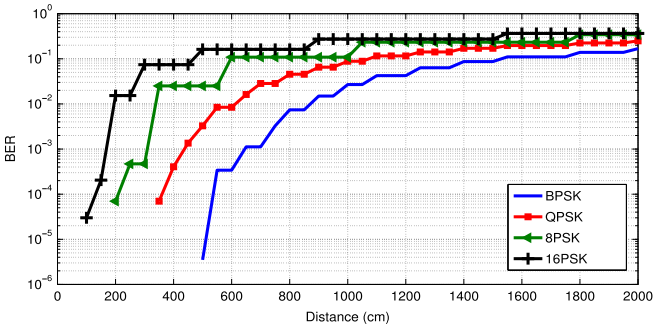

Fig. 26. Bit error rate vs. distance (cm) for modulation methods using channel C for transmission.

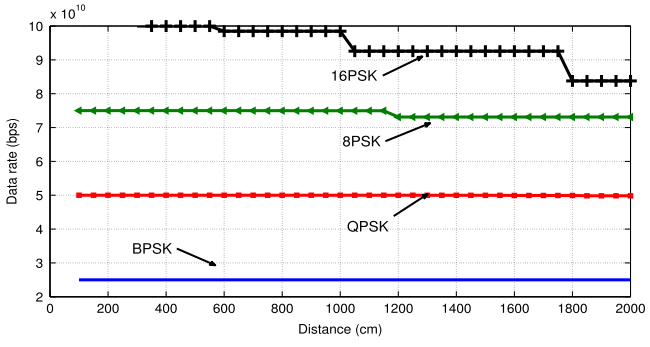

Fig. 27. Data rate (bps) vs. distance (cm) for modulation methods using channel A.

Please cite this article in press as: F. Moshir, S. Singh, Modulation and rate adaptation algorithms for terahertz channels, Nano Communication Networks (2016), http://dx.doi.org/10.1016/j.nancom.2016.07.008

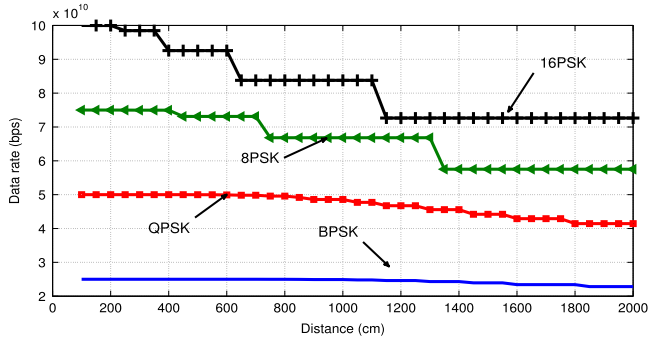

Fig. 28. Data rate (bps) vs. distance (cm) for modulation methods using channel B.

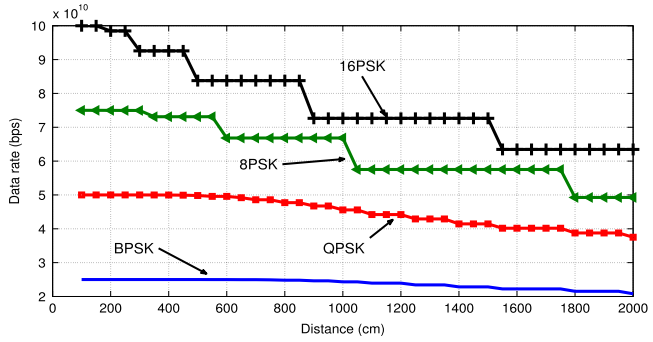

Fig. 29. Data rate (bps) vs. distance (cm) for modulation methods using channel C.

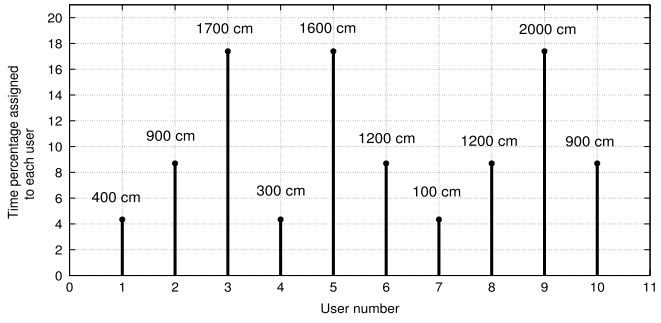

Fig. 30. The assigned time percentage to each user when channel A is used.

5.2.1. SCA simulation results

For simulation, we assume there are 10 users at different distances. Based on the result from Fig. 24, when TAP uses channel A, it can send data to users with distances up to 2000 cm with BER $<$ BER$_{Th}$. Similarly, from the result of Fig. 25, when TAP uses channel B, it covers users with distances up to 700 cm. Finally, the result from Fig. 26 shows that TAP can cover users with distances up to 500 cm using channel C.

To maintain fairness between the users, as is explained in Section 5.1, TAP assigns a time slot to each user such that all users achieve the same data rate. We set $T_{\min}$ to be 600 μs and based on that we assign the proper time slot to users.

We assign TAP-user distances of up to 2000 cm, 700 cm, and 500 cm when TAP uses channel A, B, or C, respectively. Figs. 30–32 show the percentage of time that TAP assigns to users corresponding to each scenario.

Fig. 33 shows the data rate that each user achieves, from Eqs. (18) and (19), when TAP uses channel A, B, or C. As is obvious, in all cases the fairness is maintained and all of the users achieve the same data rate. We should note that the achieved data rate for each channel depends on the average TAP-user distances.

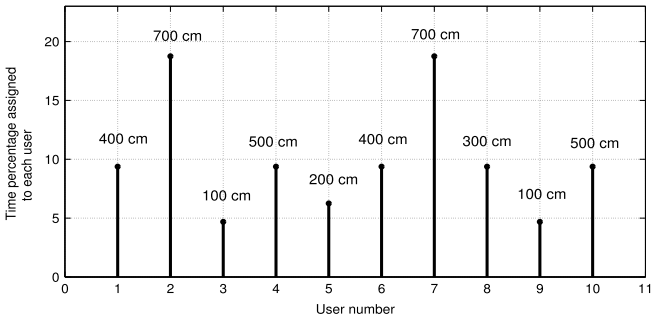

Fig. 31. The assigned time percentage to each user when channel B is used.

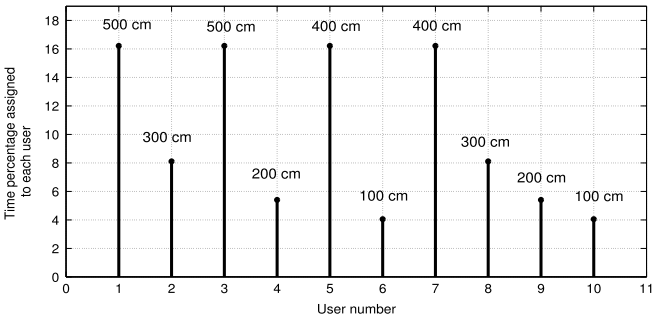

Fig. 32. The assigned time percentage to each user when channel C is used.

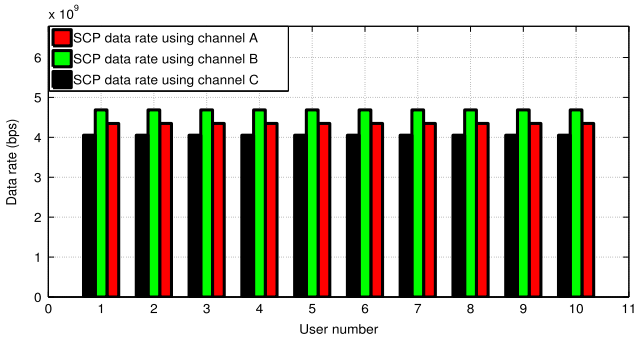

Fig. 33. SCA downlink data rate when TAP uses channel A, B, or C.

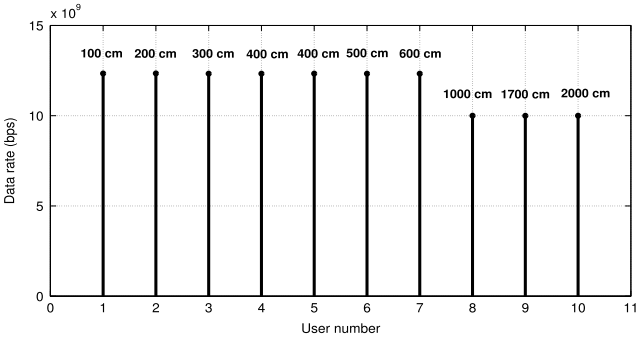

Fig. 34. MCA downlink data rate.

5.2.2. MCA simulation results

In this section we show the simulation result when using MCA. Again, we assume that we have 10 users and randomly assign TAP-user distances up to 2000 cm to them. We consider the time slot duration, T, of 200 μs. We use the MCA and run the program for 5000 time slots.

From Eqs. (20) and (21) we calculate the data rate for each user. Fig. 34 shows the achieved data rate for each user and Fig. 35 shows the percentage of time that TAP assigns to users on each channel. As

Please cite this article in press as: F. Moshir, S. Singh, Modulation and rate adaptation algorithms for terahertz channels, Nano Communication Networks (2016), http://dx.doi.org/10.1016/j.nancom.2016.07.008

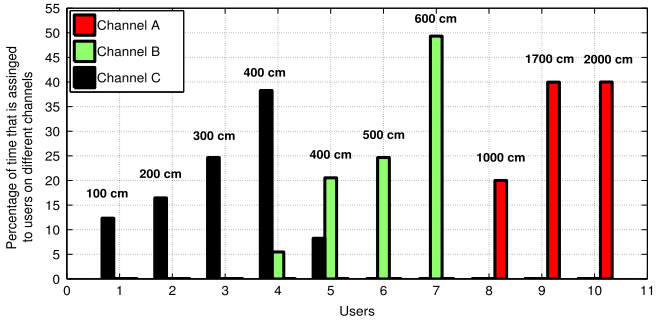

Fig. 35. The percentage of time that TAP assigns different channels to each user in MCA.

we see, users 8–10 achieve lower data rate in comparison to other users. That is, because of the long TAP-user distances, only channel A can cover these users with a low modulation order. Hence, TAP uses channel A only for these three users and their achieved data rate could not go any higher. At the same time TAP uses channel B to send data to users 4–7 and channel C for users 1–5.

6. Conclusion

In this paper we consider pulse-based and continuous wave modulation schemes for terahertz communications. For the pulse-based system, we slice the spectrum into 2 GHz bands, modulate each independently and then transmit the reconstituted pulse. For various humidity levels, we show that terabit/sec rates can be achieved in highly directional channels. The continuous wave systems we study are based on bands that are relatively immune to water absorption. We present rate adaptation algorithms for communicating using these systems when the users only have omni-directional antennas. We show that fairness can be easily achieved among competing users when frequency bands are allocated based on distance. For all of the analysis we rely on Matlab simulations where the channel model is derived based on measurements conducted using a time-domain system.

Acknowledgment

This research was funded by the NSF under award CNS-1217994.

References

[1] H.-J. Song, T. Nagatsuma, Present and future of terahertz communications, IEEE Trans. Terahertz Sci. Technol. 1 (1) (2011) 256–263.
[2] S. Cherry, Edholm's law of bandwidth, IEEE Spectr. 41 (7) (2004) 58–60. http://dx.doi.org/10.1109/MSPEC.2004.1309810.
[3] J. Federici, L. Moeller, Review of terahertz and subterahertz wireless communications, J. Appl. Phys. 107 (11) (2010).
[4] T. Kleine-Ostmann, T. Nagatsuma, A review on terahertz communications research, J. Infrared Millim. Terahertz Waves 32 (2) (2011) 143–171.
[5] T. Kürner, Towards future THz communications systems, IEEE Trans. Terahertz Sci. Technol. 5 (1) (2012).
[6] I.F. Akyildiz, J.M. Jornet, C. Han, Terahertz band: Next frontier for wireless communications, Phys. Commun. J. 12 (2014) 16–32.
[7] T. Kürner, S. Priebe, Towards THz communications-status in research, standardization and regulation, J. Infrared Millim. Terahertz Waves 35 (1) (2014) 53–62.
[8] J.F. Federici, D. Gary, R. Barat, D. Zimdars, THz standoff detection and imaging of explosives and weapons, in: Defense and Security, International Society for Optics and Photonics, 2005, pp. 75–84.
[9] D. Woolard, P. Zhao, C. Rutherglen, Z. Yu, P. Burke, S. Brueck, A. Stintz, Nanoscale imaging technology for THz-frequency transmission microscopy, Int. J. High Speed Electron. Syst. 18 (01) (2008) 205–222.
[10] J. Jornet, I. Akyildiz, Femtosecond-long pulse-based modulation for terahertz band communication in nanonetworks, IEEE Trans. Commun. 62 (5) (2014) 1742–1754.
[11] H. Song, K. Ajito, A. Hirata, A. Wakatsuki, T. Furuta, N. Kukutsu, T. Nagatsuma, Multi-gigabit wireless data transmission at over 200-GHz, in: 34th International Conference on Infrared, Millimeter, and Terahertz Waves, 2009. IRMMW-THz 2009, 2009, pp. 1–2. http://dx.doi.org/10.1109/ICIMW.2009.5325768.
[12] A. Hirata, T. Kosugi, H. Takahashi, J. Takeuchi, K. Murata, N. Kukutsu, Y. Kado, S. Okabe, T. Ikeda, F. Suginosita, et al., 5.8-km 10-Gbps data transmission over a 120-GHz-band wireless link, in: IEEE International Conference on Wireless Information Technology and Systems, (ICWITS), IEEE, 2010, pp. 1–4.
[13] I. Kallfass, J. Antes, T. Schneider, F. Kurz, D. Lopez-Diaz, S. Diebold, H. Massler, A. Leuther, A. Tessmann, All active MMIC-based wireless communication at 220 GHz, IEEE Trans. Terahertz Sci. Technol. 1 (2) (2011) 477–487.
[14] B. Zhang, Y.-Z. Xiong, L. Wang, S. Hu, A switch-based ASK modulator for 10 Gbps 135 GHz communication by 0.13 MOSFET, IEEE Microw. Wirel. Compon. Lett. 22 (8) (2012) 415–417.
[15] H. Song, K. Ajito, Y. Muramoto, A. Wakatsuki, 24 Gbit/s data transmission in 300 GHz band for future terahertz communications, Electron. Lett. 48 (15) (2012) 953–954.
[16] L. Moeller, J. Federici, K. Su, THz wireless communications: 2.5 Gb/s error-free transmission at 625 GHz using a narrow-bandwidth 1 mW THz source, in: 30th URSI General Assembly and Scientific Symposium, URSI GASS, 2011, pp. 1–4. http://dx.doi.org/10.1109/URSIGASS.2011.6050620.
[17] C. Wang, C. Lin, Q. Chen, B. Lu, X. Deng, J. Zhang, A 10-Gbit/s wireless communication link using 16-QAM modulation in 140-GHz band, IEEE Trans. Microw. Theory Tech. 61 (7) (2013) 2737–2746.
[18] B. Lu, W. Huang, C. Lin, C. Wang, A 16QAM modulation based 3 Gbps wireless communication demonstration system at 0.34 THz band, in: 38th International Conference on Infrared, Millimeter, and Terahertz Waves, (IRMMW-THz), IEEE, 2013, pp. 1–2.
[19] S. Koenig, D. Lopez-Diaz, J. Antes, F. Boes, R. Henneberger, A. Leuther, A. Tessmann, R. Schmogrow, D. Hillerkuss, R. Palmer, T. Zwick, C. Koos, W. Freude, O. Ambacher, J. Leuthold, I. Kallfass, Wireless sub-THz communication system with high data rate, Nat. Photonics 7 (2013) 977–981.
[20] C. Han, I.F. Akyildiz, Distance-aware multi-carrier (DAMC) modulation in terahertz band communication, in: IEEE International Conference on Communications, ICC, 2014, pp. 5461–5467.
[21] C. Han, A.O. Bicen, I.F. Akyildiz, Multi-wideband waveform design for distance-adaptive wireless communications in the terahertz band, IEEE Trans. Signal Process. 64 (4) (2016) 910–922.
[22] C. Han, I.F. Akyildiz, Distance-aware bandwidth-adaptive resource allocation for wireless systems in the terahertz band, IEEE Trans. Terahertz Sci. Technol. 6 (4) (2016) 541–553.
[23] A. Hirata, T. Kosugi, H. Takahashi, R. Yamaguchi, F. Nakajima, T. Furuta, H. Ito, H. Sugahara, Y. Sato, T. Nagatsuma, 120-GHz-band millimeter-wave photonic wireless link for 10-Gb/s data transmission, IEEE Trans. Microw. Theory Tech. 54 (5) (2006) 1937–1944.
[24] G. Ducournau, P. Szriftgiser, D. Bacquet, A. Beck, T. Akalin, E. Peytavit, M. Zaknoune, J. Lampin, Optically power supplied Gbit/s wireless hotspot using 1.55μm THz photomixer and heterodyne detection at 200 GHz, Electron. Lett. 46 (19) (2010) 1349–1351.
[25] C. Jastrow, S. Priebe, B. Spitschan, J. Hartmann, M. Jacob, T. Kürner, T. Schrader, T. Kleine-Ostmann, Wireless digital data transmission at 300 GHz, Electron. Lett. 46 (9) (2010) 661–663.
[26] J. Antes, J. Reichart, D. Lopez-Diaz, A. Tessmann, F. Poprawa, F. Kurz, T. Schneider, H. Massler, I. Kallfass, System concept and implementation of a mmW wireless link providing data rates up to 25 Gbit/s, in: IEEE International Conference on Microwaves, Communications, Antennas and Electronics Systems, COMCAS, 2011, pp. 1–4.
[27] X. Pang, A. Caballero, A. Dogadaev, V. Arlunno, R. Borkowski, J.S. Pedersen, L. Deng, F. Karinou, F. Roubeau, D. Zibar, et al., 100 Gbit/s hybrid optical fiber-wireless link in the w-band (75–110 GHz), Opt. Express 19 (25) (2011) 24944–24949.
[28] M. Fice, E. Rouvalis, F. van Dijk, A. Accard, F. Lelarge, C. Renaud, G. Carpintero, A. Seeds, 146-GHz millimeter-wave radio-over-fiber photonic wireless transmission system, Opt. Express 20 (2) (2012) 1769–1774.
[29] J. Antes, S. Konig, A. Leuther, H. Massler, J. Leuthold, O. Ambacher, I. Kallfass, 220 GHz wireless data transmission experiments up to 30 Gbit/s, in: IEEE MTT-S International Microwave Symposium Digest, (MTT), IEEE, 2012, pp. 1–3.
[30] K. Ishigaki, M. Shiraishi, S. Suzuki, M. Asada, N. Nishiyama, S. Arai, Direct intensity modulation and wireless data transmission characteristics of terahertz-oscillating resonant tunnelling diodes, Electron. Lett. 48 (10) (2012) 582–583.
[31] J. Antes, S. Koenig, D. Lopez-Diaz, F. Boes, A. Tessmann, R. Henneberger, O. Ambacher, T. Zwick, I. Kallfass, Transmission of an 8-PSK modulated 30 Gbit/s signal using an MMIC-based 240 GHz wireless link, in: IEEE MTT-S International Microwave Symposium Digest, IMS, 2013, pp. 1–3.
[32] S. Sarkozy, M. Vukovic, J. Padilla, J. Chang, G. Tseng, P. Tran, P. Yocom, W. Yamasaki, K. Leong, W. Lee, Demonstration of a G-band transceiver for future space crosslinks, IEEE Trans. Terahertz Sci. Technol. 3 (5) (2013) 675–681.
[33] H.-J. Song, J.-Y. Kim, K. Ajito, M. Yaita, N. Kukutsu, Fully integrated ASK receiver MMIC for terahertz communications at 300 GHz, IEEE Trans. Terahertz Sci. Technol. 3 (4) (2013) 445–452.
[34] T. Nagatsuma, S. Horiguchi, Y. Minamikata, Y. Yoshimizu, S. Hisatake, S. Kuwano, N. Yoshimoto, J. Terada, H. Takahashi, Terahertz wireless communications based on photonics technologies, Opt. Express 21 (20) (2013) 23736–23747.

Please cite this article in press as: F. Moshir, S. Singh, Modulation and rate adaptation algorithms for terahertz channels, Nano Communication Networks (2016), http://dx.doi.org/10.1016/j.nancom.2016.07.008

[35] G. Ducournau, P. Szriftgiser, A. Beck, D. Bacquet, F. Pavanello, E. Peytavit, M. Zaknoune, T. Akalin, J.-F. Lampin, Ultrawide-bandwidth single-channel 0.4-THz wireless link combining broadband quasi-optic photomixer and coherent detection, IEEE Trans. Terahertz Sci. Technol. 4 (3) (2014) 328–337.
[36] http://advancedphotonix.com/.
[37] R.M. Goody, Y.L. Yung, Atmospheric Radiation: Theoretical Basis, Oxford University Press, 1995.
[38] L. Rothman, I. Gordon, Y. Babikov, A. Barbe, D.C. Benner, P. Bernath, M. Birk, L. Bizzocchi, V. Boudon, L. Brown, et al., The HITRAN2012 molecular spectroscopic database, J. Quant. Spectrosc. Radiat. Transfer 130 (2013) 4–50.
[39] http://www.spectralcalc.com/info/CalculatingSpectra.pdf.
[40] J.H.V. Vleck, V.F. Weisskopf, On the shape of collision-broadened lines, Rev. Modern Phys. 17 (2–3) (1945) 227.
[41] Y. Yang, A. Shutler, D. Grischkowsky, Measurement of the transmission of the atmosphere from 0.2 to 2 THz, Opt. Express 19 (9) (2011) 8830–8838.
[42] H. Liebe, G. Hufford, M. Cotton, Propagation modeling of moist air and suspended water/ice particles at frequencies below 1000 GHz, in: AGARD 52nd Specialists' Meeting Electromagnetic Wave Propagation Panel, Vol. 1, 1993.
[43] J.M. Jornet, I.F. Akyildiz, Channel modeling and capacity analysis for electromagnetic wireless nanonetworks in the terahertz band, IEEE Trans. Wireless Commun. 10 (10) (2011) 3211–3221.
[44] S. Priebe, T. Kurner, Stochastic modeling of THz indoor radio channels, IEEE Trans. Wireless Commun. 12 (9) (2013) 4445–4455.
[45] J. Kokkoniemi, J. Lehtomaki, K. Umebayashi, M. Juntti, Frequency and time domain channel models for nanonetworks in terahertz band, IEEE Trans. Antennas and Propagation 63 (2) (2015) 678–691.
[46] C. Han, A.O. Bicen, I.F. Akyildiz, Multi-ray channel modeling and wideband characterization for wireless communications in the terahertz band, IEEE Trans. Wireless Commun. 14 (5) (2015) 2402–2412.
[47] A. Moldovan, M.A. Ruder, I.F. Akyildiz, W.H. Gerstacker, LOS and NLOS channel modeling for terahertz wireless communication with scattered rays, in: Globecom Workshops, (GC Wkshps), IEEE, 2014, pp. 388–392.
[48] D. Swinehart, The beer-lambert law, J. Chem. Educ. 39 (7) (1962) 333.
[49] J.K. Rhee, H. Kobayashi, W.S. Warren, Optical frequency domain differential phase shift keying in femtosecond-pulse spectral modulation systems, J. Lightwave Technol. 15 (12) (1997) 2214–2222.
[50] J.-K. Rhee, H. Kobayashi, W.S. Warren, Frequency-domain differential phase shift keying in femtosecond spread-time WDM/TDM systems, in: Conference of Information Sciences and Systems, 1996, pp. 1107–1112.
[51] Y. Yang, M. Mandehgar, D. Grischkowsky, Time domain measurement of the THz refractivity of water vapor, Opt. Express 20 (24) (2012) 26208–26218.
[52] Y. Yang, M. Mandehgar, D.R. Grischkowsky, Understanding THz pulse propagation in the atmosphere, IEEE Trans. Terahertz Sci. Technol. 2 (4) (2012) 406–415.

Farnoosh Moshir received her B.S. in computer science in 2006 and her M.S. in industrial engineering from Amirkabir university of technology, Tehran, Iran, in 2009. She also got M.S. in computer science from Portland state university, Portland, Oregon in 2014. She is currently a Ph.D. candidate in the department of computer science at the Portland state university. Her research interests include wireless networks and THz communications.

Suresh Singh is a Professor in Computer Science at Portland State University. He received his B.Tech degree from the Indian Institute of Technology, Kanpur in 1984 and Ph.D. from the University of Massachusetts at Amherst in 1990, both in Computer Science. His research interests include terahertz communication systems, green networking, communication design for the Internet of Things and information theory. He is a member of the IEEE and ACM.

Please cite this article in press as: F. Moshir, S. Singh, Modulation and rate adaptation algorithms for terahertz channels, Nano Communication Networks (2016), http://dx.doi.org/10.1016/j.nancom.2016.07.008